



Satellite-derived 1-km estimates and long-term trends of PM_{2.5} concentrations in China from 2000 to 2018

Qingqing He^{a,b,*}, Kai Gao^a, Lei Zhang^c, Yimeng Song^{d,e}, Ming Zhang^a

^a School of Resource and Environmental Engineering, Wuhan University of Technology, Wuhan 430070, China

^b Institute of Environment, Energy and Sustainability, The Chinese University of Hong Kong, Hong Kong, China

^c School of Remote Sensing and Information Engineering, Wuhan University, Luoyu Road No.129, Wuhan, China

^d Department of Land Surveying and Geo-Informatics, The Hong Kong Polytechnic University, Hong Kong, China

^e Smart Cities Research Institute, The Hong Kong Polytechnic University, Hong Kong, China

ARTICLE INFO

Handling Editor: Xavier Querol

Keywords:

Fine particulate matter (PM_{2.5})

Satellite remote sensing

Adaptive spatiotemporal modeling

Long-term trend

High spatiotemporal resolution

ABSTRACT

Exposure to ambient PM_{2.5} (fine particulate matter) can cause adverse effects on human health. China has been experiencing dramatic changes in air pollution over the past two decades. Statistically deriving ground-level PM_{2.5} from satellite aerosol optical depth (AOD) has been an emerging attempt to provide such PM_{2.5} data for environmental monitoring and PM_{2.5}-related epidemiologic study. However, current countrywide datasets in China have generally lower accuracies with lower spatiotemporal resolutions because surface PM_{2.5} level was rarely recorded in historical years (i.e., preceding 2013). This study aimed to reconstruct daily ambient PM_{2.5} concentrations from 2000 to 2018 over China at a fine scale of 1 km using advanced satellite datasets and ground measurements. Taking advantage of the newly released Multi-Angle Implementation of Atmospheric Correction (MAIAC) 1-km AOD dataset, we developed a novel statistical strategy by establishing an advanced spatiotemporal model relying on adaptive model structures with linear and non-linear predictors. The estimates in historical years were validated against surface observations using a strict leave-one-year-out cross-validation (CV) technique. The overall daily leave-one-year-out CV R² and root-mean-square-deviation values were 0.59 and 27.18 μg/m³, respectively. The resultant monthly (R² = 0.74) and yearly (0.77) mean predictions were highly consistent with surface measurements. The national PM_{2.5} levels experienced a rapid increase in 2001–2007 and significantly declined between 2013 and 2018. Most of the discernable decreasing trends occurred in eastern and southern areas, while air quality in western China changed slightly in the recent two decades. Our model can deliver reliable historical PM_{2.5} estimates in China at a finer spatiotemporal resolution than previous approaches, which could advance epidemiologic studies on the health impacts of both short- and long-term exposure to PM_{2.5} at both a large and a fine scale in China.

1. Introduction

Exposure to fine particulate matter (PM_{2.5}) has been widely acknowledged as one of the most alarming environmental threats worldwide, causing various adverse impacts on human health (Crouse et al. 2012; Pope and Dockery 2006). In 2017, ambient particulate pollution became the eighth leading lethal risk for the human body, accounting for 2940 thousand deaths globally (GBD 2018). The epidemiologic cohort studies quantitatively estimated the disease burden related to PM_{2.5} using an exposure–response function. Currently, studies focusing on exposure–response models included very few samples in areas with high risks of PM_{2.5} exposure, e.g., China (Burnett et al. 2014).

Such studies have been hindered primarily by the accurate assessment of PM_{2.5} exposure. PM_{2.5} data in China preceding 2013 are very limited, and they only became widely available after 2013 when the national ground-level air quality monitoring network initiated. Even for the PM_{2.5} dataset after 2013, most observational sites which measured the PM_{2.5} concentrations are located in urban areas, causing an uneven spatial distribution issue. Therefore, accurately describing long-term variation of ambient fine particulate matter (PM_{2.5}) at a fine spatial resolution would advance epidemiologic studies on the health impact of acute and chronic exposure to PM_{2.5} in China.

With spatially ubiquitous observations in a long-term period, satellite remote sensing has been proven an effective way to dynamically

* Corresponding author at: School of Resource and Environmental Engineering, Wuhan University of Technology, Wuhan 430070, China.

E-mail address: qqhe@whut.edu.cn (Q. He).

<https://doi.org/10.1016/j.envint.2021.106726>

Received 2 April 2021; Received in revised form 4 June 2021; Accepted 15 June 2021

Available online 25 June 2021

0160-4120/© 2021 The Authors.

Published by Elsevier Ltd.

This is an open access article under the CC BY-NC-ND license

(<http://creativecommons.org/licenses/by-nc-nd/4.0/>).

monitor atmospheric pollution through the inversion of satellite remote sensing measurements (Chudnovsky et al. 2014; Engel-Cox et al. 2004; Kloog et al. 2014; Lee et al. 2016; Li et al. 2016; Wang and Christopher 2003). A variety of schemes have been deployed to statistically associate the satellite-derived aerosol optical depth (AOD) with near-surface observations of $PM_{2.5}$ (Bai et al., 2016; Guo et al., 2017; He and Huang, 2018; Lee et al., 2016; Ma et al., 2016; Song et al., 2014; You et al., 2016; Zhan et al., 2017; Zhou et al., 2014; Fang et al., 2016). However, the statistical strategies usually require the in-situ observations as dependent input to estimate ground $PM_{2.5}$, such that their application is limited to the post-2013 period in China, during which observed constraints are available.

Driven by demands of historical $PM_{2.5}$ data, estimating $PM_{2.5}$ prior to 2013 has become an emerging attempt, using measured $PM_{2.5}$ data after 2013 and the statistically spatiotemporal autocorrelation within the data. Since $PM_{2.5}$ is interactively affected by various natural (e.g., meteorological parameters) and anthropogenic (e.g., industrial emissions) factors, the absence of measured constraints in model development usually leads to the loss of precision of historical predictions, with validated $R^2 < 0.45$ at daily timescale (Ma et al. 2016; Xiao et al. 2017). Recent studies adopted advanced statistical approaches to predict the long-term $PM_{2.5}$ sequence with improved model performance, e.g., random forest (Meng et al. 2021; Wei et al. 2021), high-dimensional expansion (Xue et al. 2019), and seasonal-GTWR model (i.e., geographically and temporally weighted regression (GTWR) model with the consideration of seasonality) (He et al. 2020). But the better performing reconstruction of historical $PM_{2.5}$ usually depends on a variety of external information such as $PM_{2.5}$ components (e.g., NO_x and SO_2) from simulation models (Meng et al. 2021; Xue et al. 2019) or emission inventory data (Wei et al. 2021), which may be limited to access, particularly for a long-term period across a large region. Besides, most

previous studies reconstructed historical $PM_{2.5}$ at coarse spatial resolutions (≥ 10 km) due to the limitation of the resolution of satellite aerosol products (Ma et al. 2016; Xue et al. 2019), or in a small study region (Liang et al. 2018; Xiao et al. 2017) due to the difficulty to capture the reasonable spatial heterogeneity in a considerably large area, or at a coarse temporal resolution (e.g., monthly scale) (Wei et al. 2021; Xiao et al. 2020). An advanced spatiotemporal model is thus needed to reconstruct long-term $PM_{2.5}$ with a high spatiotemporal resolution specifically for China, an extensive area with large heterogeneity, using independent variables that are readily available.

In the present work, we first developed a novel statistical strategy that incorporates seasonal-GTWR models with adaptive model structures to improve the accuracy of $PM_{2.5}$ predictions when $PM_{2.5}$ observations are undocumented. Meanwhile, high-resolution AOD, observed meteorological data, and surface conditions were utilized as model inputs to improve the spatiotemporal resolution of the estimates. Then, we applied the proposed modeling approach to predict daily 1-km AOD for 19 years (2000 to 2018) over the entire of China, excluding Taiwan, Macau, and Hong Kong, due to different air quality standards and data availability. Finally, we plotted a complete picture of the ambient $PM_{2.5}$ pattern in mainland China and investigated spatiotemporal patterns in $PM_{2.5}$ concentrations and exposures.

2. Materials and methods

2.1. Datasets and preprocessing

In the present work, we employed predictors such as ground $PM_{2.5}$ measurements, high-resolution AOD, surface conditions, and meteorological variables during the study period, which are similar to those in our previous study on historical $PM_{2.5}$ reconstruction over central China

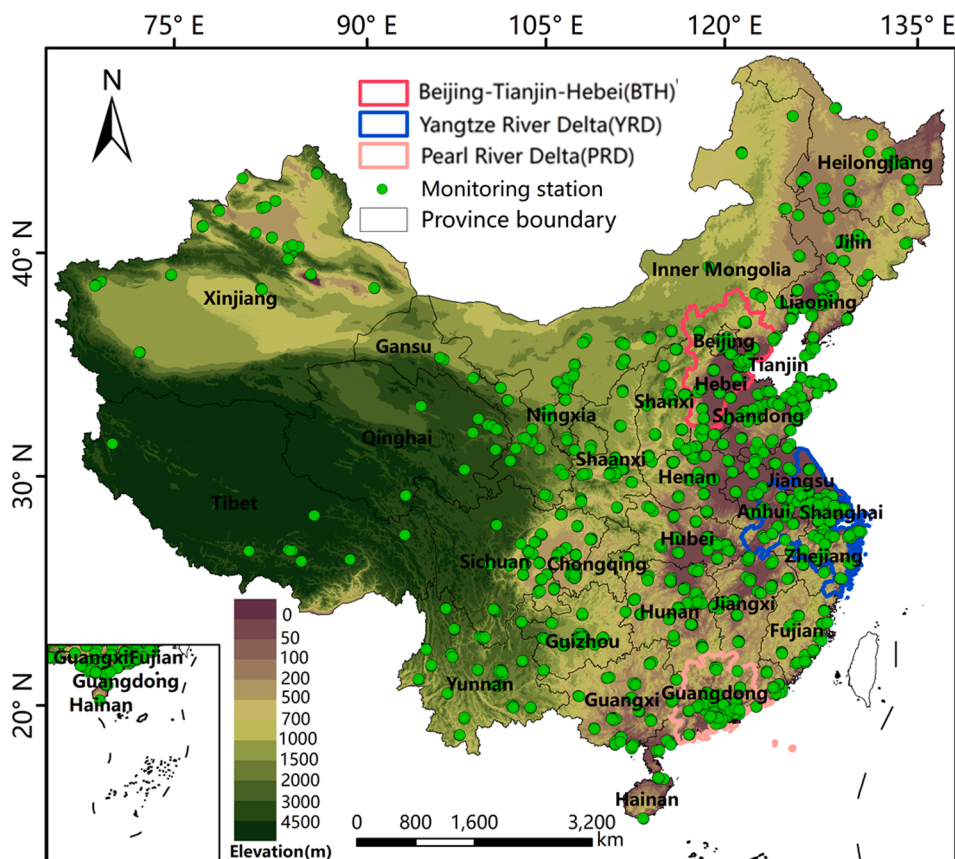


Fig. 1. Study region of the present work, showing the geolocation of the national ground-level air quality monitoring stations, three key urban agglomerations, and terrain.

from 2003 to 2018 (He et al. 2020). The data sources and integration methods involved in the modeling are briefly summarized below. For more description, please refer to He et al. (2020) and He et al. (2021).

2.1.1. Surface PM_{2.5} observations

Hourly in-situ measurements of PM_{2.5} were collected from the air quality network of the China Environmental Monitoring Center. After discarding the duplicate monitoring stations, a total of 1703 stations (Fig. 1) were distributed over mainland China during 2013–2018. The 24-hour mean PM_{2.5} concentrations were calculated by averaging the hourly PM_{2.5} data, which were used as the response variable for modeling, consistent with our previous work (He et al. 2020). We also collected the hourly measurements from the four US embassies (Beijing, Chengdu, Guangzhou, Shanghai, and Shenyang), which are the sole sources of ground PM_{2.5} observations in China before 2013 (Ma et al. 2016). These measured PM_{2.5} data were only used to evaluate the resultant PM_{2.5} other than the model inputs.

2.1.2. MAIAC 1-km AOD data

We obtained the state-of-the-art high-resolution AOD data, i.e., the Moderate-resolution Imaging Spectroradiometer (MODIS) C6 MAIAC (Multi-Angle Implementation of Atmospheric Correction) aerosol products at a spatial resolution of 1 km (MCD19A2) from the satellites Terra (2000–2018) and Aqua (2003–2018) (Lyapustin et al. 2018) as the primary predictor in historical PM_{2.5} reconstruction. According to validation results against AOD measurements from the Aerosol Robotic Network (AERONET), the MAIAC 1-km AOD data achieve a comparable accuracy with improved spatial coverage, compared with previously popular AOD products, e.g., the MODIS 10-km Dark Target (DT) and Deep Blue (DB) aerosol retrievals (Liu et al. 2019; Martins et al. 2017). With the better representation of local PM_{2.5} gradients, the MAIAC 1-km AOD dataset has been increasingly applied in particle-related studies (Liang et al. 2018; Meng et al. 2021; Wei et al. 2021; Xiao et al. 2017). In this study, both Terra and Aqua aerosol data were downloaded, and a customized fusion method was carried out to consolidate the two satellites' retrievals, which could further enlarge the number of valid daily AOD so that PM_{2.5} maps of the study area with an improved coverage can be produced (Fig. S1 in supporting information (SI)).

Because observation timespans for Aqua and Terra are different, the fusion processing was conducted separately for two periods: (1) for the period between 2003 and 2018 when both Terra and Aqua retrievals are available, and (2) for the 2000–2002 period when only Terra AOD was available (please see the details in the paragraph after Fig. S2). The comparison results in Fig. S2 show that our customized fusion method was legally feasible. Thus, the merged daily AOD was used as the primary independent variable to generate the daily fused 1-km AOD for the historical PM_{2.5} estimation.

2.1.3. Auxiliary variables

Additional predictors that can affect the PM_{2.5}-AOD relationship were used to improve the model performance including meteorological variables and surface conditions, all of which are publicly available and be easily acquired. Meteorological variables include surface temperature (T2M), relative humidity (RH), wind speed (WS), surface pressure (SP), and planetary boundary layer height (PBLH) while surface conditions include the monthly 1-km Normalized Difference Vegetation Index (NDVI) data and digital elevation model (DEM) data. Details of variables used for modeling are given in Table S1. In this study, the 1-km grid was constructed based on the MAIAC AOD. PM_{2.5} observational stations were spatially collocated to the 1-km grid cells, and those falling into one grid cell were merged. Other predictors with various spatial

resolutions were converted to match the 1-km grid cells using aggregation and interpolation techniques similar to He et al. (2020). The descriptive statistics of the sample dataset used in the adaptive spatiotemporal modeling are summarized in Table S2.

2.2. Adaptive spatiotemporal regression (ASTR) modeling and validation

Adaptive spatiotemporal regression (ASTR) modeling is an approach of dynamically modulating both the number and magnitude of independent variables as geographic area spatially varies in PM_{2.5} pollution modeling based on previous seasonal-GTWR models (He et al. 2020), which can better leverage local spatiotemporal characteristics and avoid multicollinearity problem than the previous ones. The general structure of an ASTR model incorporates response variable (i.e., ground PM_{2.5} concentration) and three types of predictors (i.e., satellite AOD, other first-order predictors, and higher-order predictors), which can be simplified as Eq. (1).

$$PM_{2.5} = AOD + Predictors^1 + Predictors^2 \quad (1)$$

where $PM_{2.5}$ represents the response variable of surface PM_{2.5} concentration; AOD is the MAIAC 1-km aerosol data denoted as the fundamental input; $Predictors^1$ are the additional variables described in Section 2.2.3 (e.g., RH, T2M, WS, and NDVI) as first-order independent variables, indicating the linear effect of auxiliary variables on the PM_{2.5}-AOD association; $Predictors^2$ are high-order predictors (e.g., AOD^2 , $AOD \times T2M$, $AOD \times WS$, $AOD \times PBLH$), representing the non-linear interaction between AOD and additional variables. According to previous studies (He et al. 2020; Xue et al. 2019), the non-linear interactions between predictors play a vital role in describing the PM_{2.5}-AOD relationship and can enhance model predictive power.

The ASTR modeling generally has three steps. First, a basic model for the entire modeling region needs to be initialized. According to the *prior* knowledge (He et al. 2020; Xue et al. 2019), the basic model for the entire study region was created with Eq. (2). The second step is to define individual modeling areas and select the best set of predictors for each modeling area. We conducted a series of multiple linear regression (MLR) models for each city/province. The optimal number of independent variables for $Predictors^1$ and $Predictors^2$ for each city/province was determined according to the MLR model performance (e.g., the coefficient of determination, significance test, and diagnosed collinearity). Geographically neighboring cities/provinces having the same set of predictors were treated as an individual modeling area for the next step of seasonal-GTWR modeling. During implementation, MLR models were conducted for cities in eastern China while for provinces in the western part because very few monitors are distributed in western cities and thus very limited samples over western cities can be used to provide spatiotemporal information. In this step, we examined all conceivable model structures over cities/provinces and compared the statistical indicators, i.e., adjusted R², variance inflation factor (VIF), and condition index, to obtain the optimal set of predictors. The last step is to construct seasonal-GTWR models based on the optimal model structure to predict historical estimates, which consider the seasonality coherent in PM_{2.5} and its covariates in the spatiotemporal weighting matrix through defining the temporal distance by cosine metric (He et al. 2020). The construction of the weighting matrix has been detailed in the previous study (He et al. 2020). The best two core parameters for each seasonal-GTWR model, i.e., the spatiotemporal bandwidth and the scaling factor between spatial and temporal distance, were ascertained according to a series of cross-validated errors (Huang et al. 2010). Fig. 2 illustrates the workflow of the reconstruction of the 1-km daily PM_{2.5} concentrations over the study area in the 2000–2018 period.

$$\begin{aligned}
 PM_{2.5st} = & \alpha_{st} + \beta_{1st} \times AOD_{st} + \beta_{2st} \times RH_{st} + \beta_{3st} \times T2M_{st} + \beta_{4st} \times WS_{st} + \beta_{5st} \times SP_{st} + \beta_{6st} \times PBLH_{st} + \beta_{7st} \times NDVI_{st} + \beta_{8st} \times DEM_s + \beta_{9st} \times AOD_{st} \\
 & \times AOD_{st} + \beta_{10st} \times AOD_{st} \times T2M_{st} + \beta_{11st} \times AOD_{st} \times RH_{st} + \beta_{12st} \times AOD_{st} \times PBLH_{st} + \beta_{13st} \times AOD_{st} \times WS_{st} + \beta_{14st} \times AOD_{st} \times T2M_{st} \\
 & + \beta_{15st} \times AOD_{st} \times SP_{st} + \beta_{16st} \times AOD_{st} \times RH_{st} \times PBLH_{st} + \varepsilon_{st}
 \end{aligned}
 \tag{2}$$

where α_{st} denotes the spatiotemporal intercept at grid cells on day t , $\beta_{1st} - \beta_{16st}$ stand for the time- and location-specific slopes for each independent variable, and ε_{st} represents the daily error term regarding location. Variables in first-order auxiliary predictors ($Predictors^1$) and higher-order predictors ($Predictors^2$) will be included for the following

modeling process or excluded from the basic model depending on the MLR performance. Then various optimal model structures can be acquired for individual seasonal-GTWR models, eventually improving the accuracy of the historical $PM_{2.5}$ predictions. For example, it may include AOD, DEM, NDVI, PBLH, RH, T2M, WS, AOD \times AOD, AOD \times RH, and AOD \times T2M as predictors for local models in Fujian province and may incorporate another group of predictors for elsewhere. During the

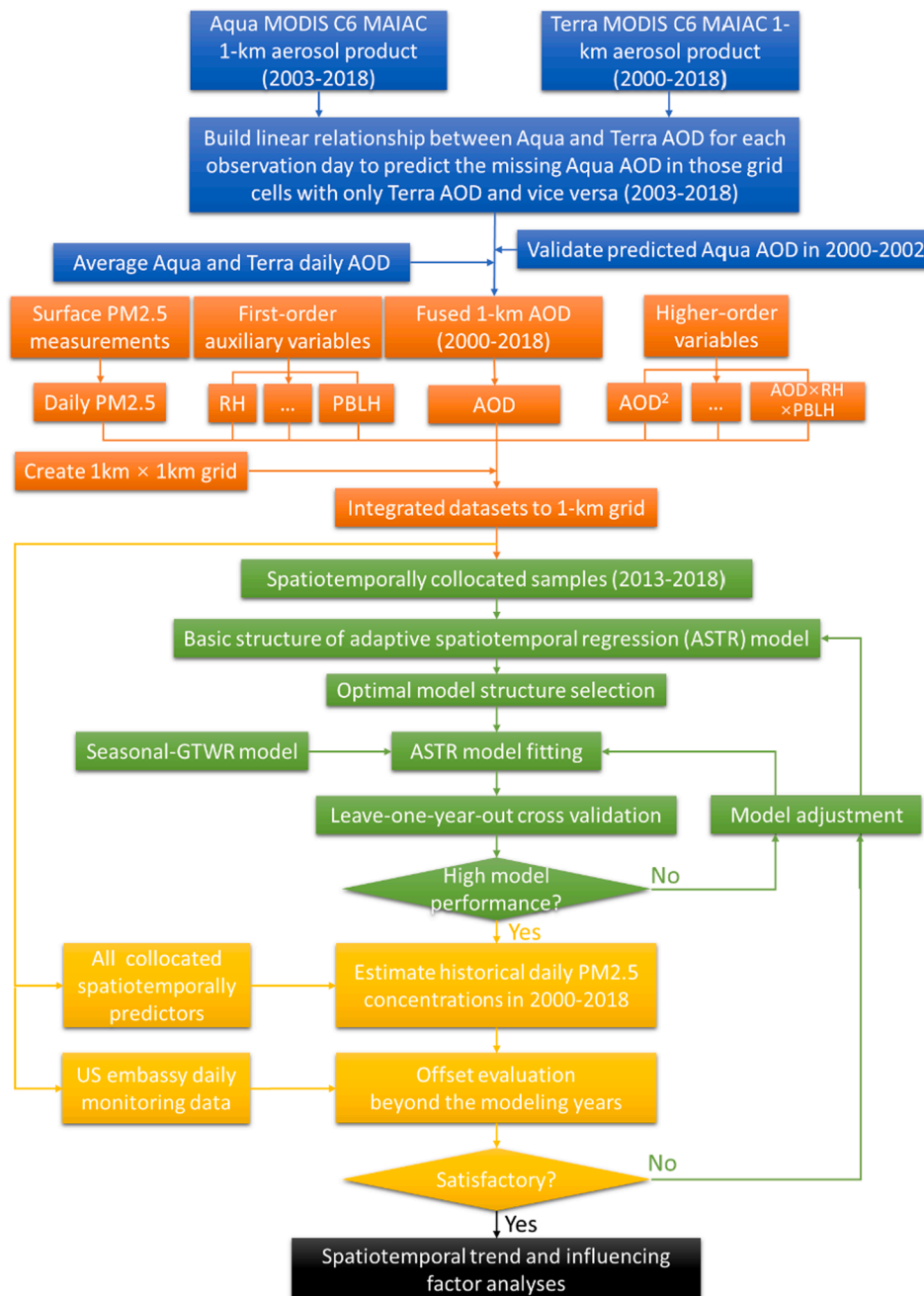


Fig. 2. The workflow of historical daily $PM_{2.5}$ prediction.

implementation, we found that RH, T2M, WS, PBLH, NDVI, and DEM were the most frequently used linear-effect variables and AOD^2 and $AOD \times T2M$ had noticeable effects on improving the $PM_{2.5}$ -AOD relationships, which were remained for most local regressions in seasonal-GTWR modeling. To avoid collinearity and enhance model performance, the collinearity indicators, i.e., VIF and condition index for independent variables, were generally required <10 and 30 in the model development.

Unlike previous studies that generally applied the temporal 10-fold CV method or used one-year data for model development and another-year data for model evaluation (Wei et al. 2021; Xiao et al. 2017), a more stringent leave-one-year-out CV (He et al. 2020; Xue et al. 2019) was applied in this study to evaluate the model's predictive power outside the modeling period. During implementation, we grouped the sample dataset by calendar year and held out a whole year of samples in each training. When the evaluation at monthly, seasonal, and yearly scales, only those averaged from $>5/30/330$ valid daily measurements a month/season/year were remained for evaluation. The linearly fitted R^2 , root mean square error (RMSE), and mean prediction error (MPE) between the predicted and measured $PM_{2.5}$ were calculated to indicate the model predictive power.

2.3. Statistical analysis methods

Both regional and pixel-based time series analysis based on general least square (GLS) regression (see details in Weatherhead et al. (1998)), was conducted to detect the long sequential $PM_{2.5}$ change. To minimize the seasonal effect within the data, we applied monthly mean $PM_{2.5}$ anomalies to the GLS regression, which were calculated by subtracting the climatological monthly mean. Such a linear trend method has been widely used in environmental analyses (Boys et al. 2014; Ma et al. 2016).

The ASTR modeling process was upgraded in MATLAB R2017 based on the basic script of the GTWR model (Huang et al. 2010). Besides, all the data analysis was conducted in MATLAB R2017. The final predictions will be available at <http://doi.org/10.5281/zenodo.4569557>.

3. Results

3.1. Validation results of model performance

Fig. 3 presents the overall results of leave-one-year-out CV for the historical $PM_{2.5}$ estimates by the ASTR model on a daily timescale. The daily high-resolution $PM_{2.5}$ estimates from the CV results were in good accordance with the daily ground measurements (CV $R^2 = 0.59$), with a daily RMSE of $27.18 \mu\text{g}/\text{m}^3$ and MPE of $17.37 \mu\text{g}/\text{m}^3$ (Fig. 3 (a)). Fig. S3 demonstrates the scatterplots of CV results at monthly and yearly scales, showing that the modeling errors decreased through averaging the estimates over time with significantly enhanced R^2 . Fig. 3 also demonstrates the critical local characteristics of our ASTR model in both temporal (Fig. 3 (b)) and spatial (Fig. 3 (c)) perspectives. For each modeling day, the resultant local R^2 value was on average of 0.76 against surface $PM_{2.5}$ average, ranging between 0.58 and 0.82. Spatially, the model performed better in eastern China (local $R^2 > 0.75$) while did poorer in western areas (local $R^2 < 0.70$), possibly due to the uneven distribution of in-situ monitors. As shown in Fig. 1, only a small number of monitors are located in western China, which provides very limited information for modeling and thus may weaken the model performance. Larger retrieval uncertainties in aerosol estimation over those areas, especially over the high-elevation area (e.g., Tibetan area) may be another reason (Lyapustin et al. 2018) for the poorer performance in the west. In general, the mean temporal local R^2 value for all grid cells was 0.78 and exceeding 86% of grid-cell local R^2 values were >0.70 . The spatial and temporal performance in each local regression generated by the ASTR model suggests that our model was reasonably stable across the large-scale modeling area and throughout the study period and explained a considerable amount of the spatiotemporal variability in the historical $PM_{2.5}$ prediction.

More importantly, we compared the monthly and yearly averages of daily historical predictions with corresponding monthly and yearly in-situ observations calculated from all measured records (i.e., including those missing AOD), and the details are summarized in Fig. 4. The monthly mean predicted $PM_{2.5}$ averaged from more than five daily predictions could be a convincingly accurate ($R^2 = 0.74$) representation of monthly actual surface $PM_{2.5}$ levels with a very slight bias (RMSE = $15.75 \mu\text{g}/\text{m}^3$ and MPE = $10.71 \mu\text{g}/\text{m}^3$). The six-day-per-month threshold is in line with the previous study of the long-term $PM_{2.5}$

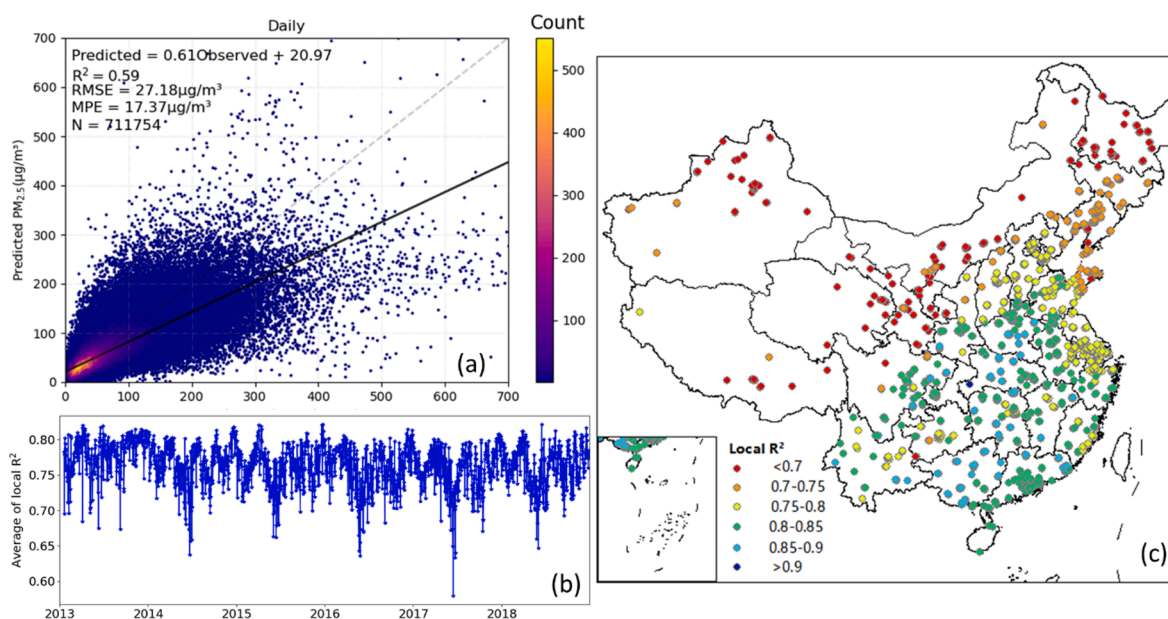


Fig. 3. The overall leave-one-year-out CV results in the study domain: (a) scatterplot, (b) time series, and (c) spatial distribution of the mean difference between estimated and measured $PM_{2.5}$.

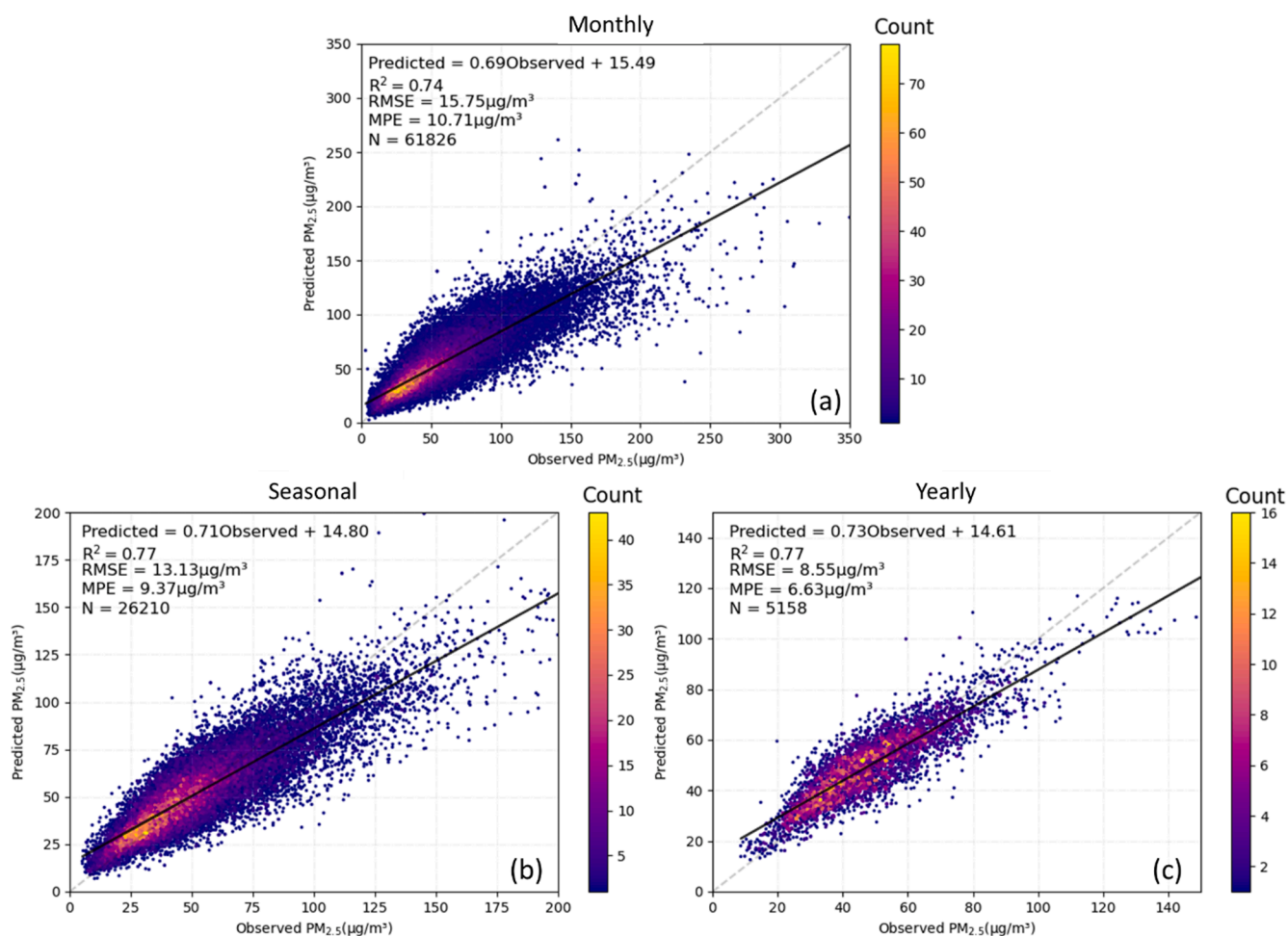


Fig. 4. Scatterplot of predicted vs. observed $\text{PM}_{2.5}$ concentrations at (a) monthly, (b) seasonal, and (c) yearly timescales. For the monthly/seasonal/yearly mean observed $\text{PM}_{2.5}$, all records from monitors, i.e., including those grid cells where satellite AOD was not available, were averaged.

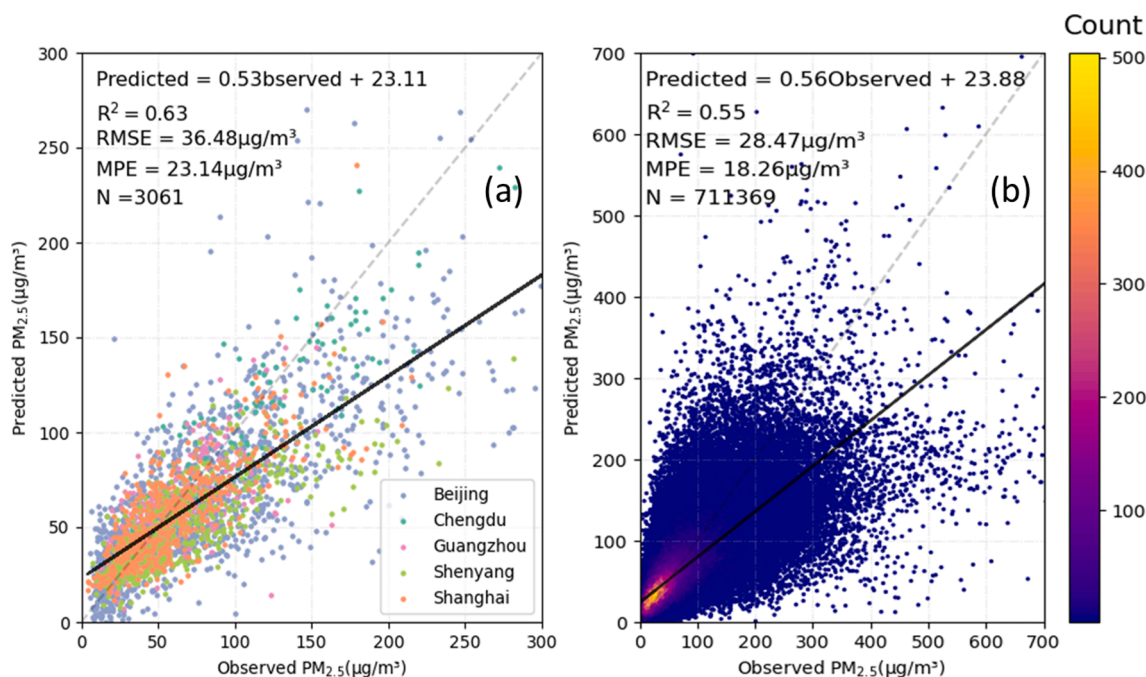


Fig. 5. Scatterplots of daily comparisons between predicted and ground $\text{PM}_{2.5}$: (a) offset comparison of $\text{PM}_{2.5}$ predictions by the ASTR model vs. US embassy measurements; (b) leave-one-year-out CV $\text{PM}_{2.5}$ results by fixed-structure GTWR model.

trend over China (Ma et al. 2016). At yearly timescale, the satellite mean $PM_{2.5}$ averaged from more than nine monthly mean predictions could accurately interpret the ground annual $PM_{2.5}$ variations with R^2 of 0.77. The annual collocated scatters overlaid with the geographic map and displayed in Fig. S4, helping us spatially pinpoint the biases between the annual mean predicted vs. observed $PM_{2.5}$, showing that a total of $\sim 60\%$ monitoring stations possessed a bias ratio of less than $\pm 15\%$. Specifically, for each validation year, there were 62%–84% of observational sites falling within the bias of $\pm 10 \mu\text{g}/\text{m}^3$, showing a good agreement with ground measurements.

To further examine the model's predictive power, offset validation using historical predictions vs. in-situ observations from the US embassy observational sites was conducted for those daily comparisons. Note that five US embassies in Beijing, Chengdu, Guangzhou, Shanghai, and Shenyang are enveloped in the study area, so that we obtained the monitoring data from the five embassy sites and used them only in model evaluation. The offset comparisons in Fig. 5(a) demonstrate a confident accuracy, with an overall R^2 of 0.63 for the total collocated points. The offset validation results in this study are also close to the previous coarse-resolution study (Xue et al. 2019), in which the national 10-km $PM_{2.5}$ data from 2000 to 2016 were reconstructed and the offset validation R^2 was reported as 0.66.

To verify our adaptive model's performance, we also developed a seasonal GTWR model with a fixed model structure as previous study (He et al. 2020) by the sample dataset used to train our ASTR model. To ensure the comparability between the fixed-structure and ASTR models, we adopted the same method and indicators as those used for ASTR models to select the optimal set of predictors but for the entire study area. AOD, DEM, NDVI, PBLH, RH, T2M, WS, and $AOD \times T2M$ were chosen as inputs for the fixed-structure model. Fig. 5(b) shows the

scatterplot and corresponding statistical error indicators of the leave-one-year-out CV results for the fixed-structure model. Compared CV results illustrated in Fig. 3(a) and (b), the ASTR model ($CV R^2 = 0.59$) demonstrates a discernible enhanced $PM_{2.5}$ predictive power with better statistical indicators than the one with fixed-structure ($CV R^2 = 0.55$). Thus, these validation results, as mentioned above, generally display that our long-term 1-km $PM_{2.5}$ predictions have been cogently evaluated (through the leave-one-year-out CV approach, directly identifying against historical offset ground-level measurements, and compared with the previous traditional modeling), which suggests a higher predictive power and prominent potential in accurately representing spatial-temporal changes of surface $PM_{2.5}$ levels.

3.2. Spatiotemporal patterns of predicted $PM_{2.5}$

Fig. 6 shows the spatiotemporal variations of the year-to-year $PM_{2.5}$ concentration during 2001–2018. In general, our long-term $PM_{2.5}$ estimates also exhibit that the spatial distribution of annual $PM_{2.5}$ averages mirrors each other and remains consistent with the multi-year pattern, in line with previous studies (Wei et al. 2021; Xue et al. 2019). Explicitly speaking, throughout the 2001–2018 period, the Taklimakan desert located in southern Xinjiang and southern Henan were the severest $PM_{2.5}$ -polluted areas, and most residents were consistently living in hazardous air with $PM_{2.5}$ loadings of $> 85 \mu\text{g}/\text{m}^3$. Other $PM_{2.5}$ -pollution hotspots included the North China Plain, Guanzhong Plain (basin area in Shanxi and Shaanxi provinces), Chengdu-Chongqing region, eastern Hunan-Hubei region, central Guangxi province, and Pearl River Delta (PRD) region, where most of the population were regularly exposed to threatening $PM_{2.5}$ levels ($>55 \mu\text{g}/\text{m}^3$). In the past 18 years, a few areas had clean air, primarily located in the less-populated region such as

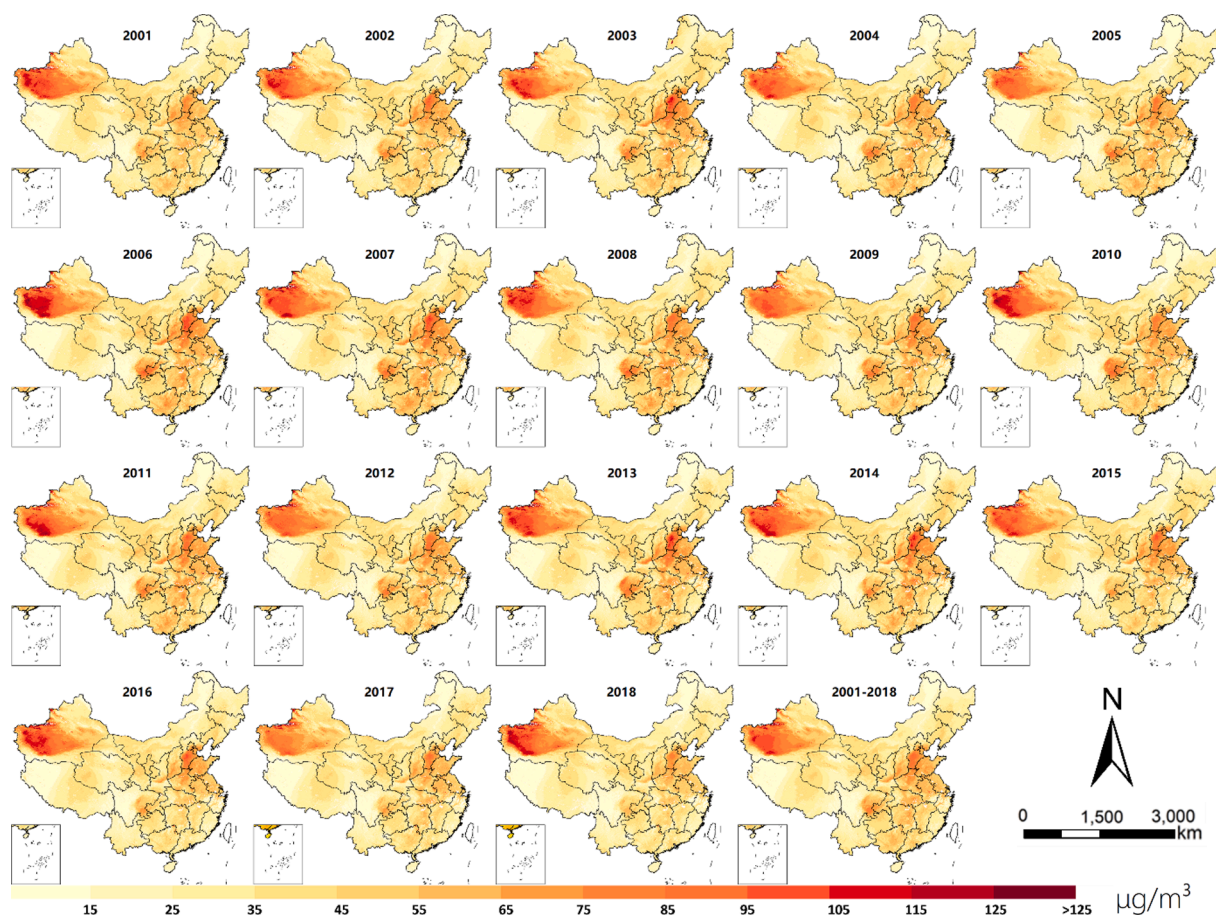


Fig. 6. Spatial distributions of 1-km $PM_{2.5}$ derived over mainland China from 2001 to 2018.

Hainan, most Tibet, western Sichuan, and northeastern Inner Mongolia, with $PM_{2.5}$ levels lower than the annual $35 \mu\text{g}/\text{m}^3$ standard.

We also look at the overall changes of $PM_{2.5}$ in the three key urban agglomerations during 2001–2018 (Fig. 6). The Beijing-Tianjin-Hebei (BTH) region was polluted the severest in 2003 ($59.99 \mu\text{g}/\text{m}^3$), followed by 2007 ($57.60 \mu\text{g}/\text{m}^3$) and 2014 ($56.52 \mu\text{g}/\text{m}^3$). The Yangtze River Delta (YRD) agglomeration was most polluted in 2011 ($47.17 \mu\text{g}/\text{m}^3$), followed by 2007 ($46.87 \mu\text{g}/\text{m}^3$) and 2008 ($46.66 \mu\text{g}/\text{m}^3$). PRD was most polluted in 2007 ($46.71 \mu\text{g}/\text{m}^3$) and cleanest in 2016 ($30.91 \mu\text{g}/\text{m}^3$) and 2018 ($32.59 \mu\text{g}/\text{m}^3$), which were the only two years in the three agglomerations satisfying the national secondary $35 \mu\text{g}/\text{m}^3$ standard.

Fig. S5 shows that seasons share a similar spatial distribution with the multi-year mean $PM_{2.5}$ pattern but possess significantly different pollution levels. The extremely severe particulate pollution with $PM_{2.5}$ concentrations higher than $105 \mu\text{g}/\text{m}^3$ occurred in spring over the Taklimakan desert. Such levels of pollution were also observed in winter over southern BTH and Guanzhong Plain. In general, our 1-km $PM_{2.5}$ predictions illustrate that the air was cleaner in warmer seasons ($PM_{2.5}$ mean value was $48.25 \mu\text{g}/\text{m}^3$ and $41.22 \mu\text{g}/\text{m}^3$ in winter and autumn, respectively) and $PM_{2.5}$ pollution was severer in colder seasons ($PM_{2.5}$ mean value was $36.33 \mu\text{g}/\text{m}^3$ and $26.58 \mu\text{g}/\text{m}^3$ for spring and summer, respectively), corresponding to previous studies (Ma et al. 2016; Wei et al. 2021).

Fig. 7 illustrates the per-pixel trends of $PM_{2.5}$ over China based on our monthly averaged time series from 2001 to 2018 using generalized least-squares regression described in Section 2.4. In general, $PM_{2.5}$ concentrations in most of China presents an overall decreasing trend ($p < 0.05$) throughout the timespan, with evident decreases occurring primarily in eastern regions, where most trends were below $-0.25 \mu\text{g}/\text{m}^3/\text{yr}$. Among those negative-trend areas, prominent decreases were observed mainly in southern provinces (e.g., Hunan, Guangxi, and Guangdong) and the Chengdu-Chongqing region, with slopes $< -0.5 \mu\text{g}/\text{m}^3/\text{yr}$ ($p < 0.05$). Pronounced negative slope ($-0.5 \mu\text{g}/\text{m}^3/\text{yr}$) was also observed in some small areas of central and northern provinces (e.g., northern Shaanxi and eastern Shanxi). However, it is worth noting that a small region in northern provinces (e.g., Shandong and Jiangsu) showed statistically upward trends, with slopes exceeding $0.25 \mu\text{g}/\text{m}^3/\text{yr}$ ($p <$

0.05), which is consistent with the previous study (Hammer et al. 2020). Moreover, most of the northern areas did not show statistically significant slopes over the 18-year study period. Over western China, statistically significant trends were found in most areas, but the strengths were a little weak, with $-0.25 \sim 0.25 \mu\text{g}/\text{m}^3/\text{yr}$ ($p < 0.05$). Fig. 7 also demonstrates that those adjacent areas generally show similar directions and statistical significances in the $PM_{2.5}$ change, indicating that the variation in $PM_{2.5}$ concentration in its neighboring areas can interact with each other.

3.3. Long-term trends of $PM_{2.5}$ exposure in China

To characterize the variation in $PM_{2.5}$ exposure, the spatial distribution of $PM_{2.5}$ was linked with gridded 1-km population data (Fu et al. 2014). According to previous studies (He et al. 2020; Xue et al. 2019), we divided the population exposure to $PM_{2.5}$ over the study region into three stages with two inflection years of 2008 and 2013 to gain insight into the temporal characteristics of ambient exposure to $PM_{2.5}$. Fig. 8 shows the national distributions of population as a function of ground $PM_{2.5}$ concentrations/trends for the 2001–2018 period. In general, for 2001, 2008, 2013, and 2018, the majority of the population in China (i.e., 79.70%, 84.99%, 84.52%, and 73.32%) has been suffering from risky $PM_{2.5}$ concentrations higher than the national secondary level limit of $35 \mu\text{g}/\text{m}^3$. Over 2001–2018, 76.37% of the total population underwent negative trends (p -value < 0.5). The proportion of the Chinese population exposed to high-level concentrations above $55 \mu\text{g}/\text{m}^3$ increasing from 27.51% in 2001 to 51.60% in 2007. During this period, 92.43% of the population experienced statistically significant positive trends. However, the proportion decreased markedly to 20.05% in 2018 as the overwhelming majority of the Chinese population experienced statistically significant negative trends in the 2013–2018 period. The long-term change of population exposed to $PM_{2.5}$ was in line with the population-weighted mean $PM_{2.5}$ (Fig. S6), which were mainly attributed to the complicated effect of economic development and air pollution control policies (Lin et al. 2018; Ma et al. 2019).

Fig. 8 also illustrates the temporal pattern of population exposure for the three agglomerations, showing the regional difference in the

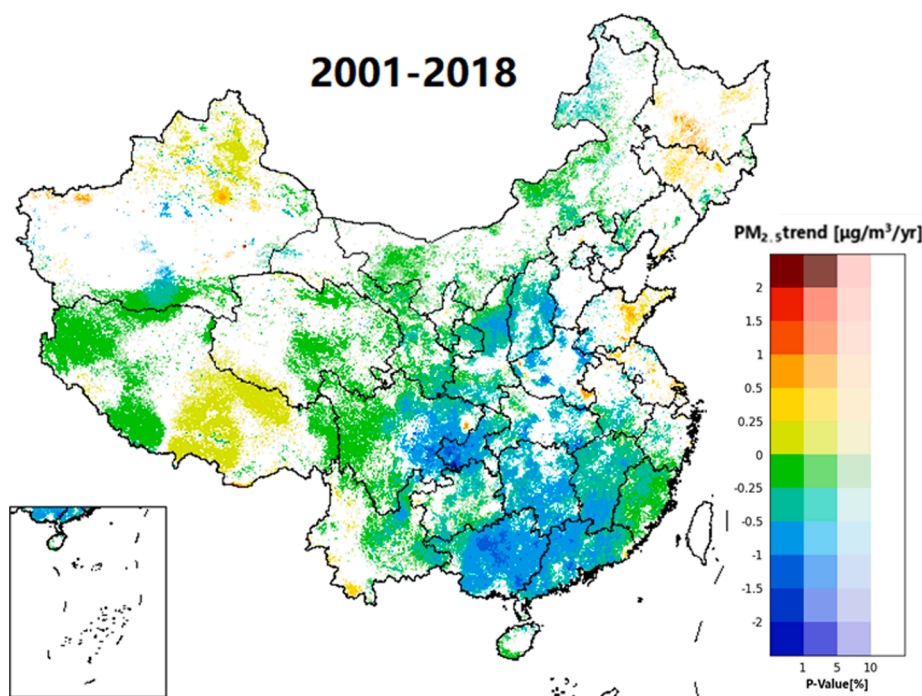


Fig. 7. Spatial maps of linear trends in monthly time series $PM_{2.5}$ anomaly from 2001 to 2018 using the generalized least-squares regression. Warm and cold color represents a positive and negative trend, respectively, and the transparency of colors represents the statistical p -value of the trends.

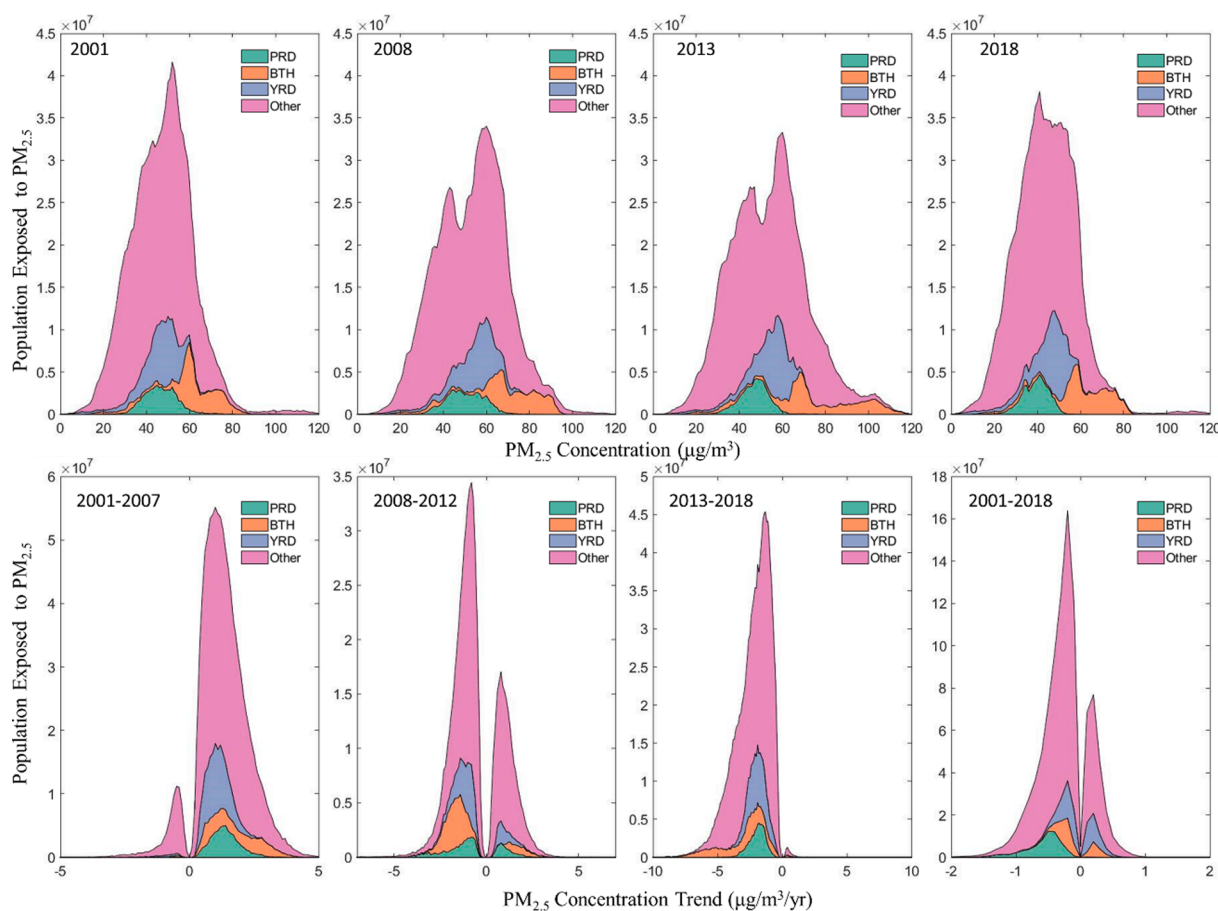


Fig. 8. Upper panel: national and regional distribution of population as a function of ground-level $PM_{2.5}$ concentration in 2001, 2008, 2013, and 2018. Lower panel: national and regional distribution of population as a function of 2001–2007, 2008–2012, 2013–2018, and 2001–2018 $PM_{2.5}$ trends with p level < 0.05; note that only statistically significant slopes (i.e., p -value < 0.05) were used to plot the population distribution against $PM_{2.5}$ trend, which means the populations in the lower panel represent those living in areas with trends' p values < 0.05 other than the total populations.

population exposed to $PM_{2.5}$ during 2001 to 2018. The BTH residents exposed to concentrations exceeding $55 \mu\text{g}/\text{m}^3$ decreased from 81.55% in 2001 to 74.08% in 2018, with 32.04% of population experiencing negative trends ($-0.3 \sim -2.0 \mu\text{g}/\text{m}^3/\text{yr}$ at p -value < 0.05). The residents of YRD exposed to high-level exposure ($>55 \mu\text{g}/\text{m}^3$) significantly increased from 9.44% in 2001 to 57.13% in 2007, while the proportion decreased noticeably to 4.07% in 2018 as more residents shifted toward $45 \sim 55 \mu\text{g}/\text{m}^3$. Compared to BTH and YRD, a small fraction (<30%) of the PRD population suffered from high-level exposures, and the fraction satisfying the national secondary standard of $35 \mu\text{g}/\text{m}^3$ increased remarkably from 6.86% in 2001 to 27.96% in 2018. The regional variation of the long-term trend of $PM_{2.5}$ population exposure was mainly due to the spatial difference in natural condition and structure of industry and energy consumption (He et al. 2021; Lin et al. 2018; Ma et al. 2019).

4. Discussion

The $PM_{2.5}$ -AOD relationship significantly varies spatiotemporally, which is too complex to describe accurately for various spatiotemporal points without observed data. Thus, it poses great challenges in deriving the historical distribution of $PM_{2.5}$ from satellite AOD because the spatiotemporal-varying relationship is hard to elucidate precisely for earlier years when in-situ $PM_{2.5}$ observations are not available. Most previous studies focusing on historical $PM_{2.5}$ estimation from satellite AOD have therefore attempted the study area in a tiny region, where less spatiotemporal variability within the data needs to be handled, compared to a large area with heterogeneous topography; even for a

small study area, the model performance (monthly CV R^2 of $0.42 \sim 0.65$) remains to be improved (Liang et al. 2018; Meng et al. 2021; Xiao et al. 2017). We proposed a novel statistical modeling scheme to quantitatively explore the deterministic relationship between ambient $PM_{2.5}$ and satellite AOD outside the modeling years, which takes into account the variation and magnitude of independent variables over both spatial and temporal perspectives. In comparison to statistical models with a fixed structure, the proposed spatiotemporal modeling with adaptive adjustments of predictors herein has a better ability to capitalize on local information in the $PM_{2.5}$ -AOD relationship, generating more accurate historical predictions of ground $PM_{2.5}$ for China (validation $R^2 = 0.74$ at monthly scale). To our knowledge, this is one of the first studies to statistically reconstruct country-wide daily $PM_{2.5}$ at a fine scale of 1 km for the historical period of 2000–2018, including the undocumented $PM_{2.5}$ -observation years.

In the traditional model settings, the structure of a statistical model is generally fixed, i.e., the predictors remain identical for the entire study area throughout the whole modeling period, e.g., the GTWR models developed by He et al. (2020), Bai et al. (2016), and Guo et al. (2017). However, a large study area may include large heterogeneity and the factors influencing $PM_{2.5}$ levels may be different from region to region. The predictors in the ASTR model developed in this study varied spatially, dependent on the statistical indicators of individual linear models. The adaptive structure allows to build a model for each region with its own set of predictors and can avoid the local collinearity issue underlying the spatiotemporal relationship to some extent, which is easily overlooked by a fixed-structure model. It thus enhances the prediction power, making it possible to generate more reliable estimates

with higher accuracy (CV $R^2 = 0.59$ (Fig. 3a) vs. 0.55 (Fig. 5b)) for the sizeable heterogeneous region.

Another strength of the present work rests with the historical time series of surface $PM_{2.5}$ at a high spatiotemporal resolution over the whole of mainland China. Due to the limitation of the spatial resolution of satellite data, previous studies only generated $PM_{2.5}$ estimates at a coarse spatial resolution (e.g., 10 km) and delivered a $PM_{2.5}$ dataset with a long temporal interval (e.g., monthly and yearly) (Ma et al. 2016; Xiao et al. 2020; Xue et al. 2019). Aided by the newly released MAIAC 1-km AOD dataset, we yielded historical 1-km $PM_{2.5}$ estimates at a daily timescale, which can successfully facilitate the tackling of $PM_{2.5}$ -related issues on a better scale. For example, the zoom-in spatial maps over the eight agglomerations during 2001–2018 in Fig. S7 present the spatial variation of $PM_{2.5}$ between cities and profile local contrast within the cities. In general, the spatial variability of $PM_{2.5}$ pollution follows the distribution of the population (Fig. S8) and difference of topography (Fig. 1), where concentrations of $PM_{2.5}$ higher than $55 \mu\text{g}/\text{m}^3$ tend to prevail in densely populated areas (e.g., the BTH, Guanzhong Plain and Chengdu-Chongqing regions) with unfavorable terrains (e.g., basin) due to more anthropogenic activities (e.g., industrial emissions, construction dust, fuel, and biomass burning) and adverse dispersion conditions (e.g., high mountains of basin margin hinder the diffusion of air pollutants). Besides illustrating the long-term trends and seasonal variations of $PM_{2.5}$, the finer-timescale sequences of population-weighted mean $PM_{2.5}$ in Fig. S7 also capture severe haze $PM_{2.5}$ -pollution episodes (e.g., extreme haze episodes frequently occurred in winter over each agglomeration, especially for those sustaining a long time and involving several regions, e.g., in 2008 and 2013 (Wang et al. 2014)). These findings indicate that our predicted data can elucidate characteristics of historical $PM_{2.5}$ on a finer spatiotemporal scale, which will benefit further air-pollution and epidemiologic studies on both short-term and long-term timescales in urban areas.

A few previous studies have examined the predictive power of statistical models in forecasting the historical daily $PM_{2.5}$. Here, we compared our model outputs with previous studies' results (Table 1). Due to the differences in research domains between studies, we averaged our CV estimates to weekly and monthly scales and extracted subsets to collocate spatiotemporal scopes with previous studies to ensure a fair comparison. The comparison results in Table 1 suggest that the historical estimates in this study were better than, or at least comparable to, the predictions in previous studies in both the model accuracy and spatial resolutions. For instance, Xue et al. (2019) applied the same validation approach as the one in this study, i.e., the leave-one-year-out CV method, to validate the model predictive power; the respective CV R^2 value was reported as 0.61 and 0.71 for daily and monthly scale, close to ours. However, our fine-resolution estimates can better represent the particle gradient and promote local-scale study than their coarse-resolution ones. On the other hand, compared to CV R^2

reported by Wei et al. (2021), our estimates show lower model accuracy. The difference probably comes from different validation schemes adopted between the two studies. Instead of the leave-one-year-out CV approach used in the present work, they used one-year data modeling and another-year data testing. Liang et al. (2018)' predictions (Table 1) show the difference in the validated monthly R^2 over two specific years can be as large as 0.13, suggesting that the one-year-data testing method may not be a complete assessment of the overall predictive power in inferring the historical $PM_{2.5}$ for a statistical model. Besides, those previous studies incorporated more predictors than what we applied to the model setting in this study, such as $PM_{2.5}$ components from emission inventory or cloud fraction (Meng et al. 2021; Wei et al. 2021; Xue et al. 2019). For the long-term $PM_{2.5}$ reconstruction, these measures are not always publicly and easily available in a large-scale area. Only upon publicly available inputs, our approach could be readily applied to other regions and deliver historical estimates with confident precision comparable to those from other approaches.

Based on historical 1-km estimates, we explored the spatiotemporal pattern and trends of $PM_{2.5}$ in China at multiple spatial and temporal scales, providing a complete picture for dramatic changes in $PM_{2.5}$ pollution experienced by China over the recent decades. With the speedy economic development and urbanization, China experienced a swift increase in $PM_{2.5}$ level over the first decade of the 21st century ($1.08 \mu\text{g}/\text{m}^3/\text{yr}$ in Fig. 8), which were primarily occurred in the densely populated eastern area while almost no visible change happened in the west (Fig. 6). To fight the air pollution problem, a series of policies and measures to reduce air pollutant emissions have been enforced from 2006 onwards, successfully shifting the upward trend over eastern China and making it begin to decrease significantly, especially since 2013 (Fig. 6 and Fig. S6). These findings indicate that it is scientifically reasonable to continuously exert strict emission control/restriction policies on eastern China and even stricter; however, it seems not enough. Due to arid and semi-arid surface conditions (Fig. S10), $PM_{2.5}$ levels in northwestern China maintained extremely high throughout the study timespan (Fig. 6) and showed a slight change in recent years (Fig. S9 and Fig. S6). Although less population live in the northwest (Fig. S8), $PM_{2.5}$ pollution has transboundary interactions across urban administrative boundaries (Fig. 7) and can be transported over long distances, suggesting that cities/regions need additional actions to improve the air quality countrywide collaboratively.

The major limitation of this work originated from the lack of historical $PM_{2.5}$ observations. Although we used a spatiotemporal modeling method to better leverage the temporal information in the $PM_{2.5}$ -AOD relationship, we could not directly quantify the historical relationship. Based on the state-of-the-art validation method of the leave-one-year-out CV, we evaluated the uncertainty in our predictions; however, it is also an indirect way to quantify the estimates' errors. Also, Fig. S1 suggests that this study remains challenged by the AOD missingness

Table 1

Comparison of the leave-one-year-out CV estimates from the ASTR model with previous results in the literature.

Validation of historical $PM_{2.5}$ predictions in previous studies						Validated R^2 in this study
Study	Spatial		Temporal		CV R^2	
	Domain	Scale	Period	Scale		
Ma et al. 2016	China	$0.1 \times 0.1^\circ$	Jan-Jun, 2014	Daily	0.41	0.59
Xiao et al., 2017	YRD	$1 \times 1 \text{ km}$	2015	Monthly	0.73	0.74
Liang et al., 2018	Beijing*	$1 \times 1 \text{ km}$	2013	weekly	0.48	0.56
Wei et al. 2019	China	$1 \times 1 \text{ km}$	2014	Monthly	0.42	0.74
Xue et al., 2019	China	$0.1 \times 0.1^\circ$	2016	Monthly	0.55	0.64
			leave-one-year-out CV	Daily	0.55	0.61
				Monthly	0.61	0.59
Meng et al., 2021	Northeastern China	$1 \times 1 \text{ km}$	Leave-one-year-out CV	Daily	0.71	0.71
				Monthly	0.50	0.51
				Monthly	0.62	0.63
Wei et al., 2021	China	$1 \times 1 \text{ km}$	–	Monthly	0.80	0.71

* A rectangular area around Beijing between 114° – 118.5° in longitude and 38° – 42° in latitude.

issue, although we have used the best-available aerosol product and a fusion method to improve the daily spatial coverage. The uncertainty attributed to the missing data issue was quantitatively assessed by comparing annual mean biases in satellite-derived vs. ground-observed PM_{2.5} concentrations (Fig. S4). Although existing difference, the statistical bias for comparisons based on all observed PM_{2.5} in Fig. 4, with a monthly R² of 0.79 and the seasonal value of 0.82, was a little larger than those with only valid AOD (R² of 0.75 for monthly and 0.77 for seasonal) in Fig. S11, also suggesting that our predictions are generally reliable and can be further applied to PM_{2.5}-related study.

5. Conclusion

This study presented a newly spatiotemporal modeling framework to quantitatively describe the historical relationship between ground PM_{2.5} and satellite AOD for mainland China by fully characterizing the local spatiotemporal information using adaptive model structures, which combine linear effects and non-linear interactions between predictors. Through a strict evaluation method of leave-one-year-out CV, the adaptive estimator has been evidenced as trustworthy in inferring ambient PM_{2.5} beyond the modeling period, with better accuracy than previous statistical approaches. Upon this method and the fused MAIAC 1-km AOD data, a high-quality PM_{2.5} dataset with a high spatial resolution of 1 km grid was generated for China from 2000 to 2018 for the first time. Our long-term PM_{2.5} predictions show that most of China suffered from risky PM_{2.5} exposure, particularly in densely populated urban agglomerations such as the BTH region. The national PM_{2.5} levels experienced a rapid increase in 2001–2007 and switched to decline significantly between 2013 and 2018. Most of the discernable decreasing trends occurred in eastern and southern areas, while air quality in western China changed slightly in the recent two decades. Our estimates are promising to bridge knowledge gaps concerning exposure–response models in seriously PM_{2.5} polluted air, which is essential to advance studies on the health burden of both short-term and long-term exposure to PM_{2.5} in China and to support further research on a complete assessment of the effectiveness of PM_{2.5} alleviation measures and policies and warrant further studies.

CRedit authorship contribution statement

Qingqing He: Conceptualization, Data curation, Methodology, Software, Validation, Writing - original draft, Writing - review & editing. **Kai Gao:** Visualization, Writing - review & editing. **Lei Zhang:** Software. **Yimeng Song:** Writing - review & editing. **Ming Zhang:** Writing - review & editing.

Declaration of Competing Interest

The authors declare that they have no known competing financial interests or personal relationships that could have appeared to influence the work reported in this paper.

Acknowledgment

This study is supported by the National Natural Science Foundation of China (Grant NO. 41901324) and the Fundamental Research Funds for the Central Universities (WUT: 203208002). We thank the Supercomputing Center of Wuhan University for supporting part of numerical calculations. We also acknowledge Qingyue Open Environmental Data Center (<https://data.epmap.org>) for providing part of air pollution data.

Appendix A. Supplementary material

Supplementary data to this article can be found online at <https://doi.org/10.1016/j.envint.2021.106726>.

References

- Bai, Y., Wu, L., Qin, K., Zhang, Y., Shen, Y., Zhou, Y., 2016. A geographically and temporally weighted regression model for ground-level pm_{2.5} estimation from satellite-derived 500 m resolution aod. *Remote Sensing* 8 (3), 262. <https://doi.org/10.3390/rs8030262>.
- Boys, B.L., Martin, R.V., van Donkelaar, A., MacDonell, R.J., Hsu, N.C., Cooper, M.J., Yantosca, R.M., Lu, Z., Streets, D.G., Zhang, Q., Wang, S.W., 2014. Fifteen-year global time series of satellite-derived fine particulate matter. *Environmental science & technology* 48 (19), 11109–11118.
- Burnett, R.T., Pope, C.A., Ezzati, M., Olives, C., Lim, S.S., Mehta, S., Shin, H.H., Singh, G., Hubbell, B., Brauer, M., Anderson, H.R., Smith, K.R., Balme, J.R., Bruce, N.G., Kan, H., Laden, F., Prüss-Ustün, A., Turner, M.C., Gapstur, S.M., Diver, W.R., Cohen, A., 2014. An integrated risk function for estimating the global burden of disease attributable to ambient fine particulate matter exposure. *Environmental health perspectives* 122 (4), 397–403.
- Chudnovsky, A.A., Koutrakis, P., Kloog, I., Melly, S., Nordio, F., Lyapustin, A., Wang, Y., Schwartz, J., 2014. Fine particulate matter predictions using high resolution aerosol optical depth (aod) retrievals. *Atmospheric Environment* 89, 189–198.
- Crouse, D.L., Peters, P.A., van Donkelaar, A., Goldberg, M.S., Villeneuve, P.J., Brion, O., Khan, S., Atari, D.O., Jerrett, M., Pope, C.A., Brauer, M., Brook, J.R., Martin, R.V., Stieb, D., Burnett, R.T., 2012. Risk of nonaccidental and cardiovascular mortality in relation to long-term exposure to low concentrations of fine particulate matter: A canadian national-level cohort study. *Environmental health perspectives* 120 (5), 708–714.
- Engel-Cox, J.A., Holloman, C.H., Coutant, B.W., Hoff, R.M., 2004. Qualitative and quantitative evaluation of modis satellite sensor data for regional and urban scale air quality. *Atmospheric Environment* 38 (16), 2495–2509.
- Fang X, Li R, Xu Q, Bottai M, Fang F, Cao Y. 2016. A two-stage method to estimate the contribution of road traffic to pm_{2.5} concentrations in beijing, china. *International journal of environmental research and public health* 13:124.
- Fu, J., Jiang, D., Huang, Y., 2014. Km grid population dataset of china (populationgrid_china). Global Change Research Data Publishing & Repository.
- GBD Collaborators. 2018. Global, regional, and national comparative risk assessment of 84 behavioural, environmental and occupational, and metabolic risks or clusters of risks for 195 countries and territories, 1990–2017: A systematic analysis for the global burden of disease study 2017. *Lancet* (London, England) 392:1923.
- Guo, Y., Tang, Q., Gong, D.-Y., Zhang, Z., 2017. Estimating ground-level pm_{2.5} concentrations in beijing using a satellite-based geographically and temporally weighted regression model. *Remote Sensing of Environment* 198, 140–149.
- Hammer, M.S., van Donkelaar, A., Li, C., Lyapustin, A., Sayer, A.M., Hsu, N.C., Levy, R. C., Garay, M.J., Kalashnikova, O.V., Kahn, R.A., Brauer, M., Apte, J.S., Henze, D.K., Zhang, L.i., Zhang, Q., Ford, B., Pierce, J.R., Martin, R.V., 2020. Global estimates and long-term trends of fine particulate matter concentrations (1998–2018). *Environmental Science & Technology* 54 (13), 7879–7890.
- He, Q., Huang, B., 2018. Satellite-based mapping of daily high-resolution ground pm_{2.5} in china via space-time regression modeling. *Remote Sensing of Environment* 206, 72–83.
- He, Q., Zhang, M., Song, Y., Huang, B., 2021. Spatiotemporal assessment of pm_{2.5} concentrations and exposure in china from 2013 to 2017 using satellite-derived data. *Journal of Cleaner Production* 286, 124965. <https://doi.org/10.1016/j.jclepro.2020.124965>.
- Huang, B., Wu, B., Barry, M., 2010. Geographically and temporally weighted regression for modeling spatio-temporal variation in house prices. *International Journal of Geographical Information Science* 24 (3), 383–401.
- Kloog, I., Chudnovsky, A.A., Just, A.C., Nordio, F., Koutrakis, P., Coull, B.A., et al., 2014. A new hybrid spatio-temporal model for estimating daily multi-year pm_{2.5} concentrations across northeastern USA using high resolution aerosol optical depth data. *Atmospheric Environment* 95, 581–590.
- Lee, H.J., Chatfield, R.B., Strawa, A.W., 2016. Enhancing the applicability of satellite remote sensing for pm_{2.5} estimation using modis deep blue aod and land use regression in california, united states. *Environmental science & technology* 50, 6546–6555.
- Li, Z., Zhang, Y., Shao, J., Li, B., Hong, J., Liu, D., et al., 2016. Remote sensing of atmospheric particulate mass of dry pm_{2.5} near the ground: Method validation using ground-based measurements. *Remote sensing of environment* 173, 59–68.
- Liang, F., Xiao, Q., Wang, Y., Lyapustin, A., Li, G., Gu, D., Pan, X., Liu, Y., 2018. Maiac-based long-term spatiotemporal trends of pm_{2.5} in beijing, china. *Science of The Total Environment* 616–617, 1589–1598.
- Lin, C., Liu, G., Lau, A., Li, Y., Li, C., Fung, J., et al., 2018. High-resolution satellite remote sensing of provincial pm_{2.5} trends in china from 2001 to 2015. *Atmospheric Environment* 180, 110–116.
- Liu, N., Zou, B., Feng, H., Wang, W., Tang, Y., Liang, Y.u., 2019. Evaluation and comparison of multiangle implementation of the atmospheric correction algorithm, dark target, and deep blue aerosol products over china. *Atmospheric Chemistry and Physics* 19 (12), 8243–8268.
- Lyapustin, A., Wang, Y., Korkin, S., Huang, D., 2018. Modis collection 6 maiac algorithm. *Atmospheric Measurement Techniques* 11.
- Ma, Z., Hu, X., Sayer, A.M., Levy, R., Zhang, Q., Xue, Y., et al., 2016. Satellite-based spatiotemporal trends in pm_{2.5} concentrations: China, 2004–2013. *Environmental health perspectives* 124, 184–192.
- Ma, Z., Liu, R., Liu, Y., Bi, J., 2019. Effects of air pollution control policies on pm_{2.5} pollution improvement in china from 2005 to 2017: A satellite-based perspective. *Atmospheric Chemistry and Physics* 19, 6861–6877.

- Martins, V.S., Lyapustin, A., Carvalho, L.A.S., Barbosa, C.C.F., Novo, E.M.L.M., 2017. Validation of high-resolution maiaac aerosol product over south america. *Journal of Geophysical Research: Atmospheres* 122 (14), 7537–7559.
- He Q, Gu Y, Zhang M. 2020. Spatiotemporal trends of pm2. 5 concentrations in central china from 2003 to 2018 based on MAIAC-derived high-resolution data. *Environment International* 137:105536.
- Meng X, Liu C, Zhang L, Wang W, Stowell J, Kan H, et al. 2021. Estimating pm2.5 concentrations in northeastern china with full spatiotemporal coverage, 2005-2016. *Remote Sensing of Environment* 253:112203.
- Pope, C.A., Dockery, D.W., 2006. Health effects of fine particulate air pollution: Lines that connect. *Journal of the Air & Waste Management Association* 56 (6), 709–742.
- Song, W., Jia, H., Huang, J., Zhang, Y., 2014. A satellite-based geographically weighted regression model for regional pm 2.5 estimation over the pearl river delta region in china. *Remote Sensing of Environment* 154, 1–7.
- Wang, J., Christopher, S.A., 2003. Intercomparison between satellite-derived aerosol optical thickness and pm2.5 mass: Implications for air quality studies. *Geophysical Research Letters* 30.
- Wang, Y., Yao, L., Wang, L., Liu, Z., Ji, D., Tang, G., Zhang, J., Sun, Y., Hu, B., Xin, J., 2014. Mechanism for the formation of the january 2013 heavy haze pollution episode over central and eastern china. *Science China Earth Sciences* 57 (1), 14–25.
- Weatherhead, E.C., Reinsel, G.C., Tiao, G.C., Meng, X.-L., Choi, D., Cheang, W.-K., Keller, T., DeLuisi, J., Wuebbles, D.J., Kerr, J.B., Miller, A.J., Oltmans, S.J., Frederick, J.E., 1998. Factors affecting the detection of trends: Statistical considerations and applications to environmental data. *Journal of Geophysical Research: Atmospheres* 103 (D14), 17149–17161.
- Wei J, Huang W, Li Z, Xue W, Peng Y, Sun L, et al. 2019. Estimating 1-km-resolution PM2. 5 concentrations across China using the space-time random forest approach. *Remote Sensing of Environment*. 231:111221.
- Wei J, Li Z, Lyapustin A, Sun L, Peng Y, Xue W, et al. 2021. Reconstructing 1-km-resolution high-quality pm2. 5 data records from 2000 to 2018 in china: Spatiotemporal variations and policy implications. *Remote Sensing of Environment* 252:112136.
- Xiao, Q., Wang, Y., Chang, H.H., Meng, X., Geng, G., Lyapustin, A., et al., 2017. Full-coverage high-resolution daily pm2.5 estimation using maiaac aod in the yangtze river delta of china. *Remote Sensing of Environment* 199, 437–446.
- Xiao, Q., Geng, G., Liang, F., Wang, X., Lv, Z., Lei, Y.u., Huang, X., Zhang, Q., Liu, Y., He, K., 2020. Changes in spatial patterns of PM2.5 pollution in China 2000–2018: Impact of clean air policies. *Environment International* 141, 105776. <https://doi.org/10.1016/j.envint.2020.105776>.
- Xue, T., Zheng, Y., Tong, D., Zheng, B., Li, X., Zhu, T., et al., 2019. Spatiotemporal continuous estimates of pm2.5 concentrations in china, 2006-2016: A machine learning method with inputs from satellites, chemical transport model, and ground observations. *Environment International* 123, 345–357.
- You, W., Zang, Z., Zhang, L., Li, Y.i., Pan, X., Wang, W., 2016. National-scale estimates of ground-level pm2. 5 concentration in china using geographically weighted regression based on 3 km resolution modis aod. *Remote Sensing* 8 (3), 184. <https://doi.org/10.3390/rs8030184>.
- Zhan, Y., Luo, Y., Deng, X., Chen, H., Grieneisen, M.L., Shen, X., et al., 2017. Spatiotemporal prediction of continuous daily pm2.5 concentrations across china using a spatially explicit machine learning algorithm. *Atmospheric Environment* 155, 129–139.
- Zhou, Q., Jiang, H., Wang, J., Zhou, J., 2014. A hybrid model for pm 2.5 forecasting based on ensemble empirical mode decomposition and a general regression neural network. *Science of the Total Environment* 496, 264–274.